DAΦNE TECHNICAL NOTE

INFN - LNF, Accelerator Division

Frascati, March 26, 1996

Note: **MM-12**

MEASUREMENTS ON ANSALDO SEXTUPOLE PROTOTYPE FOR THE DAΦNE MAIN RINGS (LARGE SEXTUPOLE)

B. Bolli, N. Ganlin, F. Iungo, M. Paris, M. Preger, C. Sanelli, F. Sardone, F. Sgamma, M. Troiani

1. Introduction

The first prototype of the Main Rings sextupoles (Large Sextupole), built by ANSALDO Energia, Genova, has been delivered to LNF on December 5, 1995. The magnet has been immediately tested and the results of the measurements are reported in the following.

The clearance between the magnet and the achromat vacuum vessel was checked by mounting the magnet on the arc vacuum chamber. This test put in evidence that the external dimensions of the excitation coils were out of tolerance: a minimum clearance of 87.5 mm between coil and coil was therefore requested to ANSALDO. With this modification, the magnet was accepted and the release for series production given to ANSALDO on December 18th.

The sextupole was designed by LNF staff and Fig. 1 shows a picture of the magnet. Figure 2a gives the lamination profile, while Fig. 2b is an expanded view of the pole profile. Table I lists the coordinates of the lamination and pole profiles. Table II gives the main parameters of the sextupole magnet.

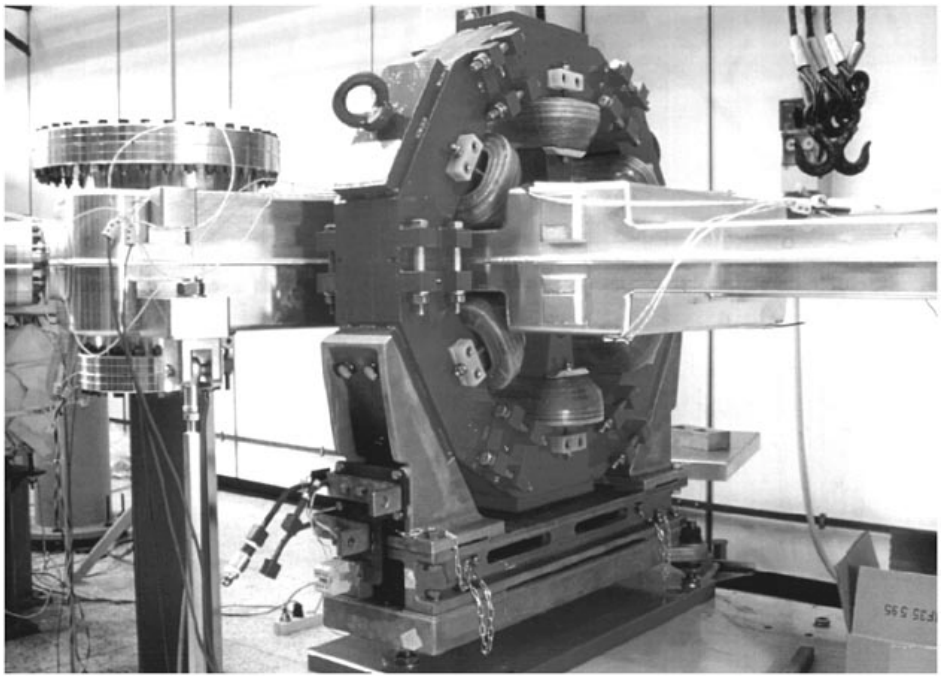

Figure 1 - Sextupole prototype assembled on its vacuum chamber

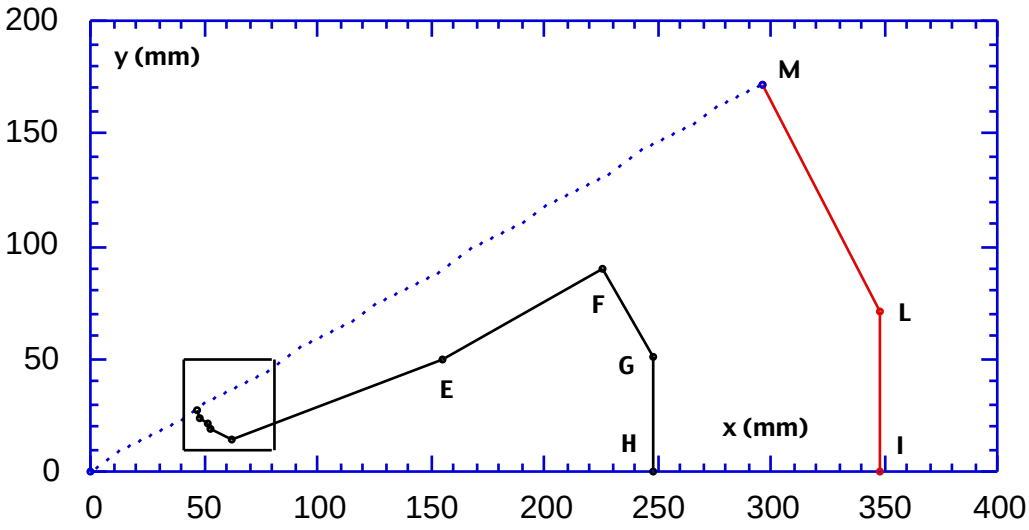

Figure 2a - Sextupole lamination profile

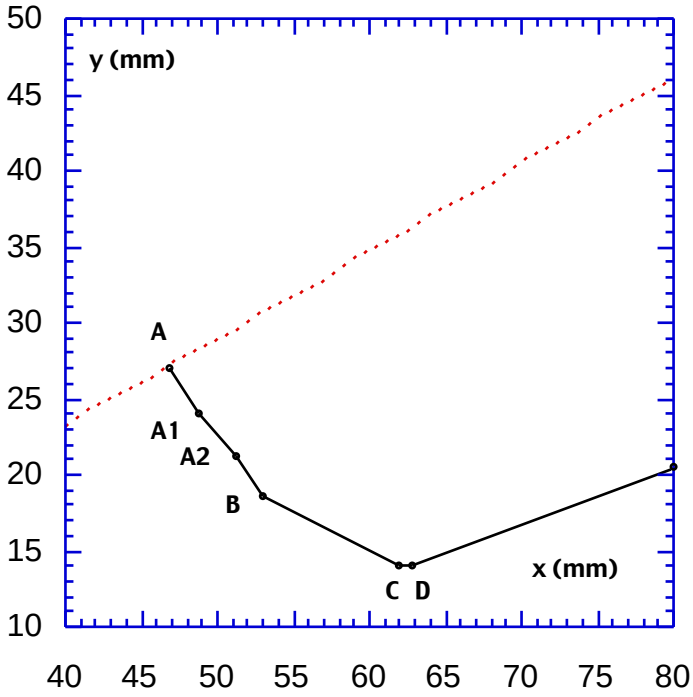

Figure 2b - Expanded view of the pole profile

Table I - Pole Profile Coordinates

Point	x (mm)	y (mm)
A	46.76	27.00
A1	48.73	24.10
A2	51.24	21.30
B	53.00	18.58
C	61.85	13.98
D	62.85	13.98
E	155.40	49.32
F	226.00	90.08
G	248.00	50.44
H	248.00	0.0
I	348.00	0.0
L	348.00	70.78
M	296.66	171.28

Table II - Sextupole prototype parameters.

Operating point	units	Nominal	Maximum
Gradient	T/m^2	90	234
Magnet Bore radius	mm	54	54
Magnetic Length (av)	mm	153	151
Good Field Region	mm	±30	±30
Turns Per Pole		24	24
Current	A	78.3	209.3
Current Density	A/mm^2	2.48	6.34
Copper Conductor	mm x	7x7	7x7
Cooling Hole Diameter	mm	4.5	4.5
Resistance per Magnet	m Ω	41.6	41.6
Inductance per Magnet	mH	6	6
Voltage per Magnet	V	3.25	8.7
Power	W	254.5	1821
Water Circuit per Magnet		2	2
Total water per Magnet	L/s	0.04	0.04
Pressure Drop	ATM	2.4	2.4
Water Temperature Rise	°C	1.5	10

2. Electrical measurements

The resistance of the sextupole was measured by means of a micro-ohm-meter (AOIP mod. OM 20) at room temperature. The measured value was 41.5 mΩ at 21 °C against the theoretical value of 40.4 mΩ. The same measurement was accomplished by using the Volt-Ampere method and the following data were measured:

8.71 V @ 209.3 A, corresponding to 41.6 mΩ

this value was obtained at the same room temperature as in the previous measurement. The agreement between the results obtained with the two different methods is very good.

The inductance and resistance of the sextupole were also measured by means of a LCR meter (LCR meter HP 4284 A) at different frequencies. The results are shown in Fig. 3. The corresponding dc values can be extrapolated from these data. They are consistent with the measured and design data.

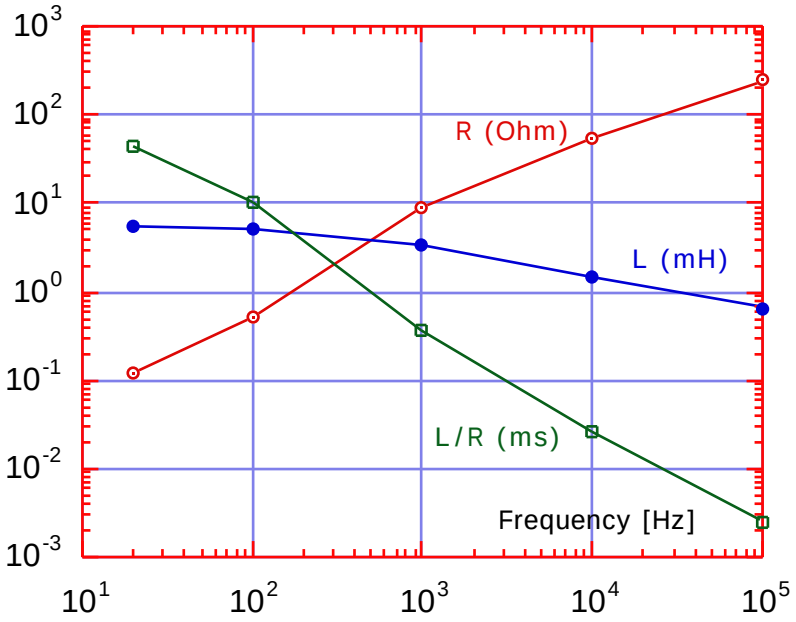

Figure 3 - Resistance, Inductance and time constant versus frequency

3. Magnetic measurements

The dependence of the sextupole gradient at the magnet center on the excitation current has been measured by means of the 4 axes computer controlled Hall probe system of the magnetic measurements laboratory [1]. The vertical component of the field B (Tesla) has been measured at ±30 mm from the magnet axis on the horizontal symmetry plane. The central gradient, defined as the second derivative of the field, is derived as:

$$S = \partial^2 B/\partial x^2 = (B_{+30} + B_{-30})x(10^4/9)$$

and is shown in Fig. 4 as a function of the excitation current.

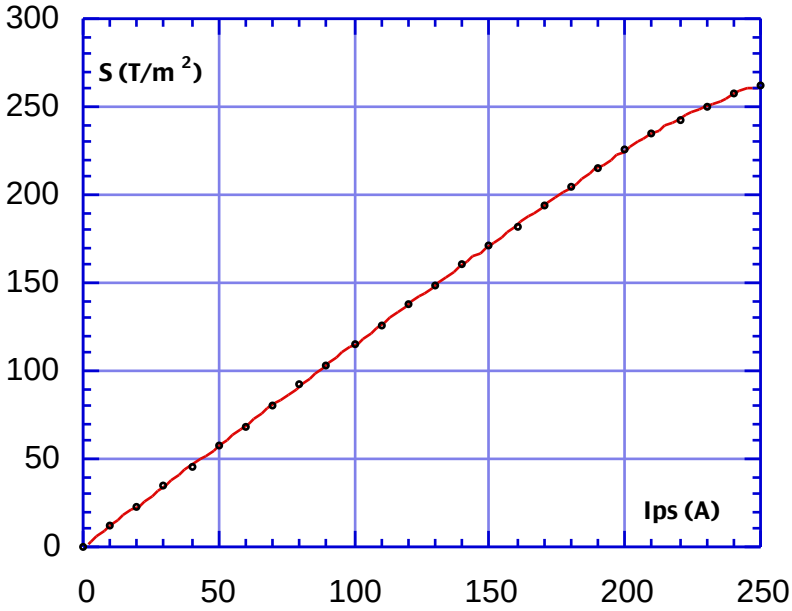

Figure 4. Sextupole gradient versus excitation current

With the Hall probe system we have measured also the vertical field component on the horizontal symmetry plane along straight lines parallel to the magnet axis. The field has been measured up to a distance of 300 mm on both sides in steps of 10 mm in the longitudinal direction. The scans have been performed with two different excitation currents (78.3 and 209.3 A) at horizontal distances from the magnet axis of ±10, ±20, ±30 and ±40 mm. Figure 5 shows the behaviour of the field as a function of the longitudinal position at the four horizontal distances from the axis on the positive side at the higher excitation current.

The field integral along each longitudinal scan for the two currents is also shown in Fig. 6. The magnetic length, defined as the field integral divided by the field at the magnet center (where it reaches its maximum value) is given in Fig. 7, on an expanded scale. The slight asymmetry between right and left is compatible with the overall positioning accuracy of the Hall probe.

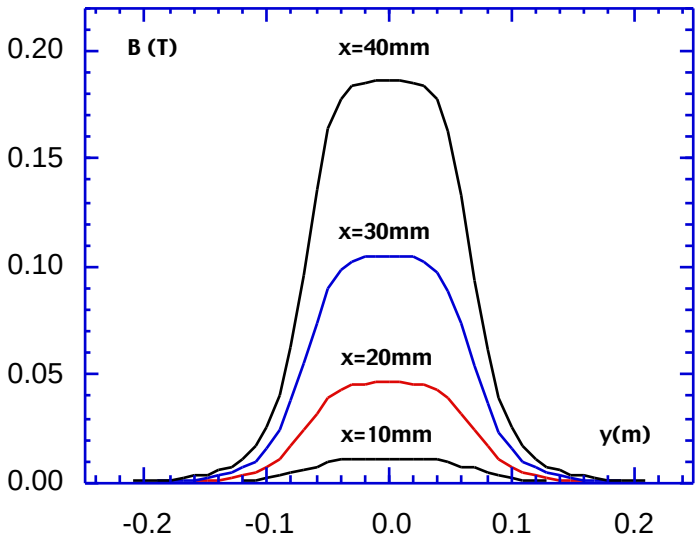

Figure 5. Vertical field component along straight lines parallel to the magnet axis on the horizontal symmetry plane (Ips = 209.3 A)

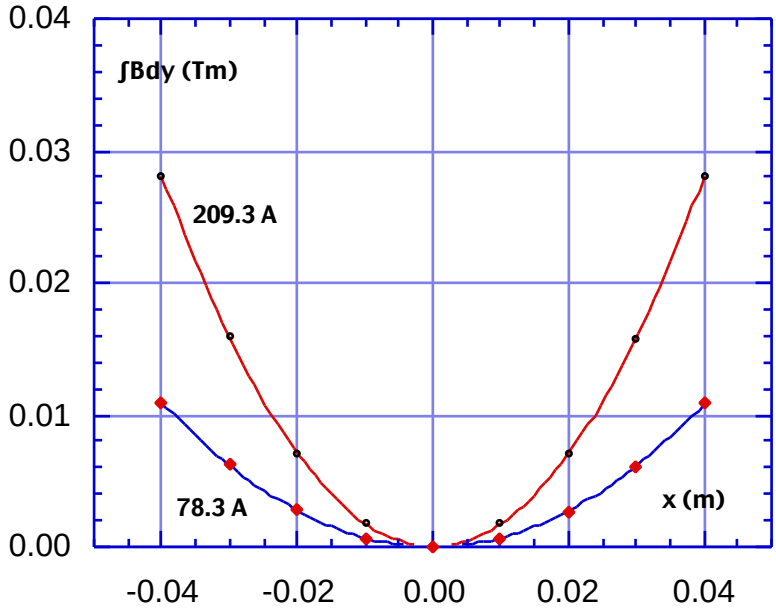

Figure 6. Field integral versus horizontal distance from magnet axis

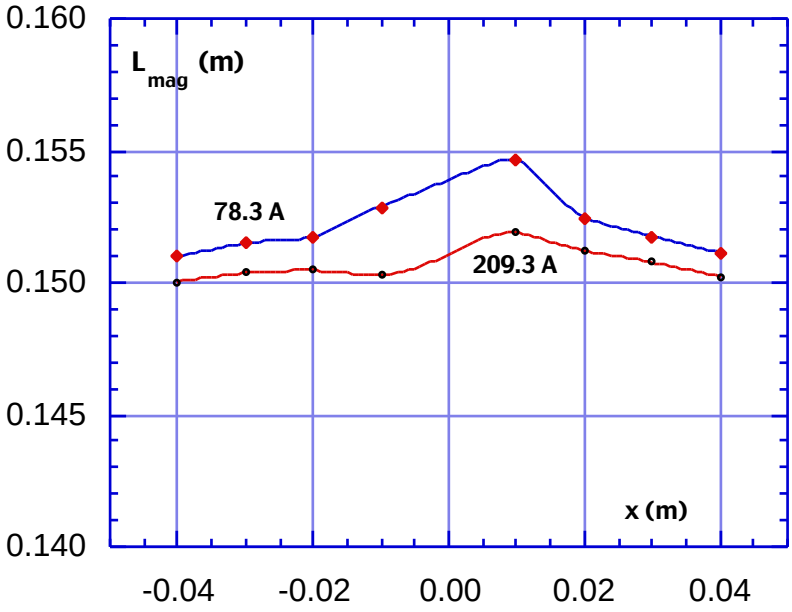

Figure 7. Magnetic length versus horizontal distance from magnet axis (expanded scale).

The integrated sextupole gradient and the contributions of higher order terms to the field have been measured with the rotating coil system [1] in steps of ≈10A up to the maximum operating current. At the end of this procedure, the magnet has been opened on the horizontal plane, in order to simulate the insertion of the vacuum chamber, closed again and few measurements repeated.

Figure 8 shows the integrated gradient before opening the magnet. The difference between these values and those measured after splitting is very small at low currents, but becomes not negligible at higher current (≈0.2% at the maximum current. Figure 9 shows the fractional difference between the two measurements.

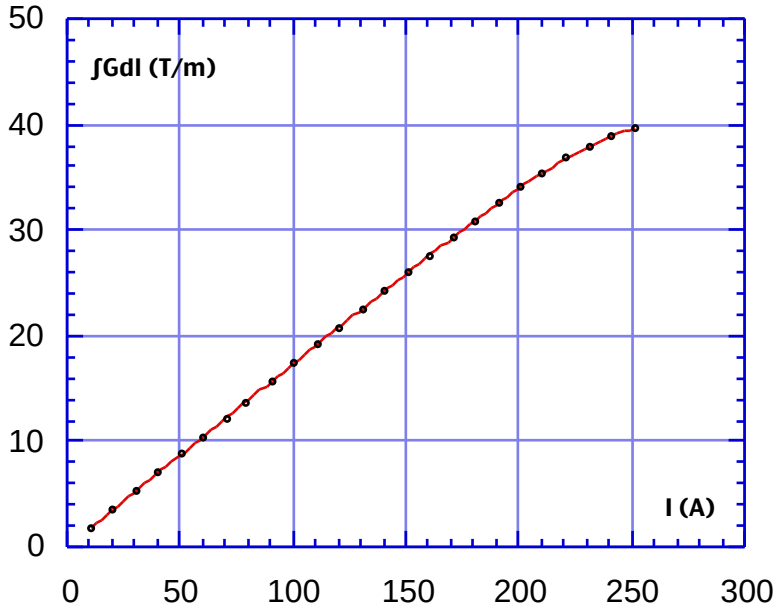

Figure 8. Integrated sextupole gradient versus excitation current

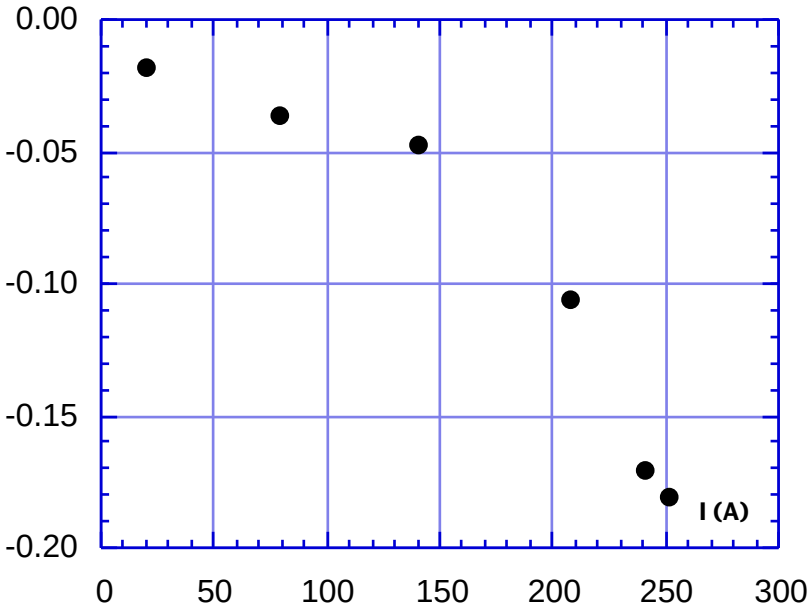

Figure 9. Fractional difference between integrated gradient values before and after splitting

Another important figure of merit for the field quality estimate is the deviation of the measured field with respect to the ideal sextupole on a circle with the radius of the nominal good field region (30 mm). This quantity is obtained from the rotating coil system output by summing up all the higher order contributions separately for the azimuthal and radial components, taking their vector sum and dividing by the main sextupole component, in steps of two degrees along the azimuthal coordinate. The result is the overall deviation from the ideal field, and it is shown in the form of a plot such as that shown in Fig. 10.

From the periodicity of the components it is clear that the main contribution to the overall deviation comes from the 18-th pole, which is the main systematic multipole with the same symmetry of the sextupole. The average deviation from the ideal field is the average value of the upper solid curve |B| in Fig. 10.

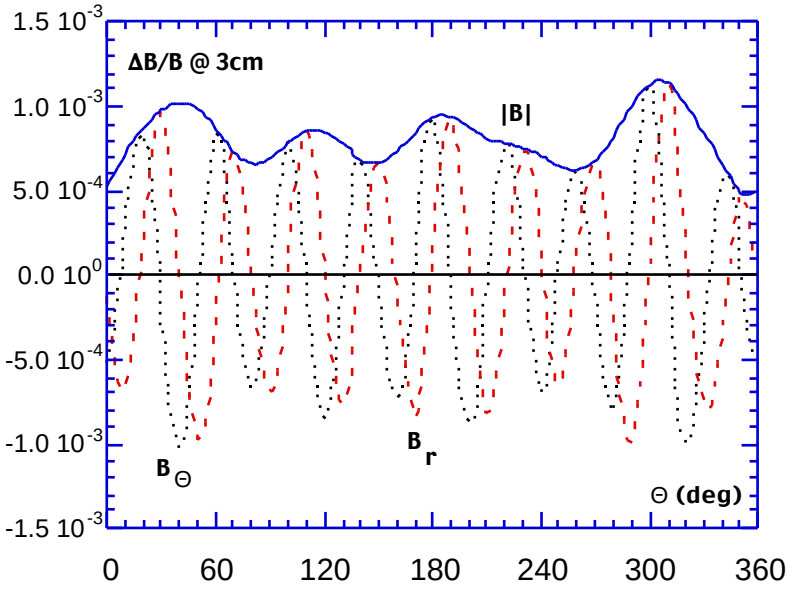

Figure 10. Field quality of the sextupole prototype (Ips = 120.62 A)

Figure 11 shows, on an expanded scale, the variation of the average field deviation with the excitation current (dots interpolated by the solid line). The isolated squares are the values measured after splitting the magnet. A slight degradation at high and low current can be observed; the degradation, however, was reduced after opening and closing the magnet.

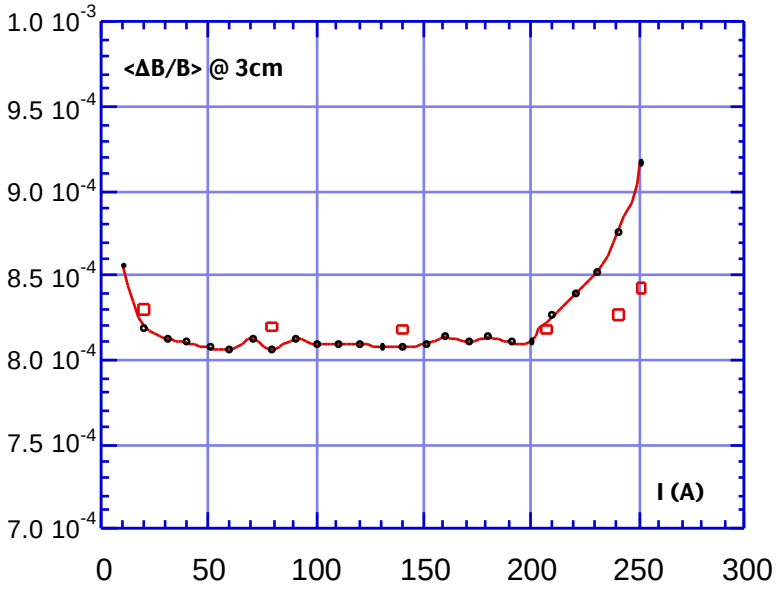

Figure 11. Average deviation from the ideal field at the boundary of the good field region (dots before splitting, squares after splitting)

It can be seen from the rotating coil system output, that the most important high order harmonic contributions to the field deviation (larger than 10^{-4} at the boundary of the good field region) are the octupole, decapole, 12-pole and 18-pole, the latter being the largest one.

Figure 12 shows on an expanded scale the 18-pole divided by the main sextupole component at 30 mm from the sextupole axis as a function of the excitation current. In this case, neglecting the first point at very low excitation current, the contribution does not depend on the excitation current. As expected, it is a systematic deviation which comes from the pole profile, and its phase is always opposite to the main sextupole one.

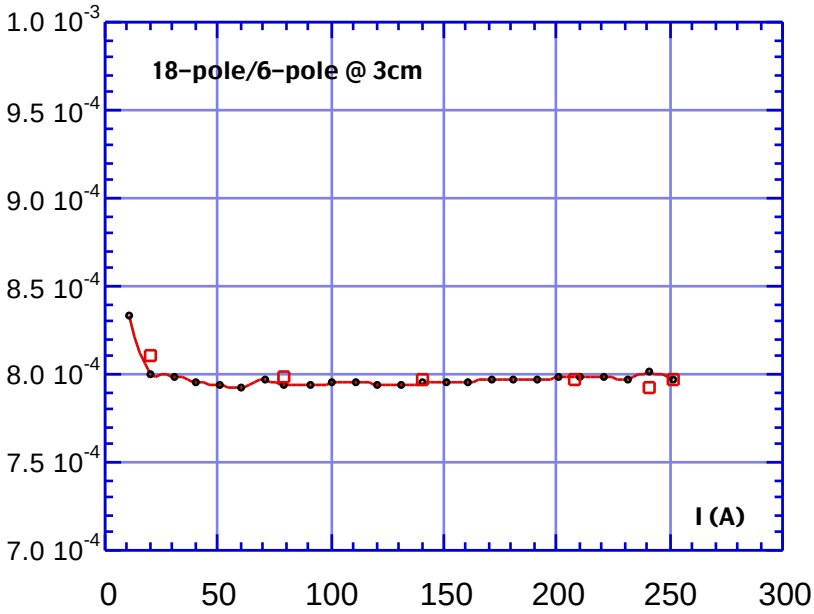

Figure 12. 18-pole/Sextupole at the boundary of the good field region
(dots before splitting, squares after splitting)

The contributions of the other high order terms are much smaller, although not negligible. Figure 13 gives the 12-pole, always divided by the sextupole at 30 mm from the axis. The behaviour is similar to the 18-pole, but ≈5 times smaller. The 12-pole contribution is in phase with the sextupole.

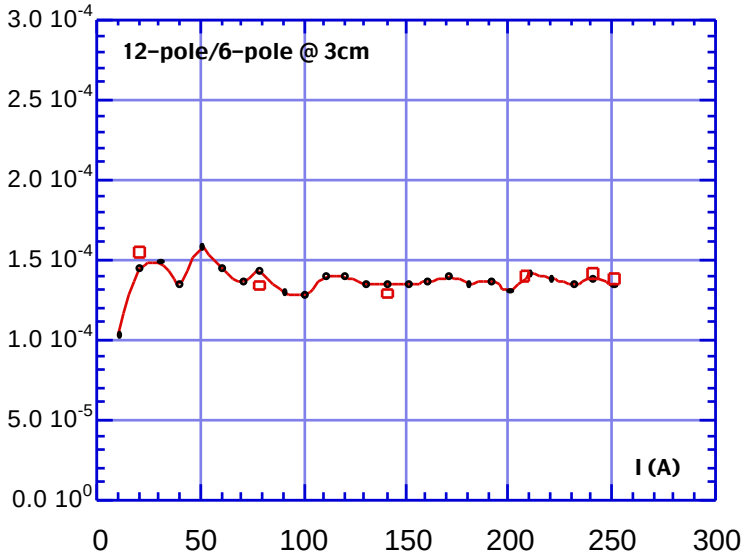

Figure 13. 12-pole/Sextupole at the boundary of the good field region
(dots before splitting, squares after splitting)

Figure 14 shows the behaviour of the decapole component. Before splitting the magnet there seems to be a rather strong fluctuation, within a factor of two, at low current. The fluctuation seems to reduce between the points measured after splitting, although the number of measured points is rather small. As discussed in detail in [2], the measured value of the high order component should be larger than the sensitivity of the measuring system, estimated to be around 0.5×10^{-4} for this component. The phase with respect to the sextupole component varies between -55 and -20 degrees.

Figure 15 plots the contribution of the octupole component. In this case the expected sensitivity is $\approx 0.7 \times 10^{-4}$. The points at low current (except the first one) are in the order of the expected sensitivity, so that the fluctuation in not relevant (the phase fluctuates over a wide range as well). There is a sharp increase of the octupole term in the saturation region, somewhat reduced after splitting. It is clear that the degradation of the average field deviation at high current (see Fig. 11) comes from the octupole contribution.

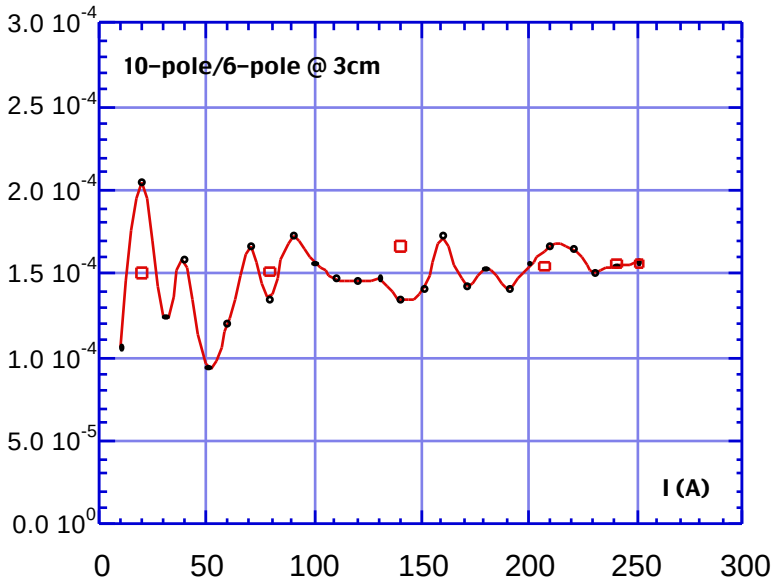

Figure 14. 10-pole/Sextupole at the boundary of the good field region (dots before splitting, squares after splitting)

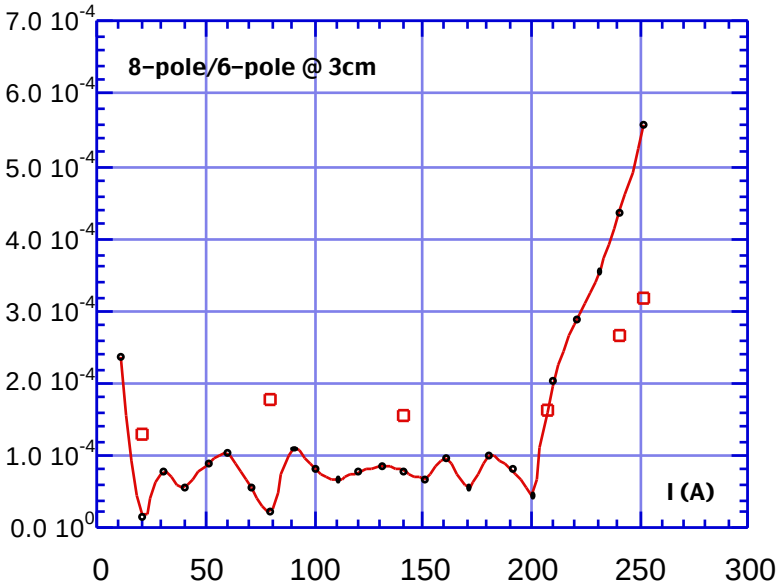

Figure 15. Octupole/Sextupole at the boundary of the good field region (dots before splitting, squares after splitting)

4. Mechanical measurements

The rotating coil system is insensitive to tilts of the magnetic axis with respect to the coil one. For this reason we have developed a mechanical alignment system that defines the direction of the magnet mechanical axis; we can reasonably assume that the mechanical and magnetic axes are parallel.

The alignment system consists of a precision machined cylinder, with the same radius as the sextupole bore, which leans on the three lower poles. An optical target on each side of the cylinder defines the mechanical axis of the magnet. A precision machined table, equipped with two slides driven by micrometric movements in the horizontal plane, leans on three pins inserted in three holes realised on the top surface of the magnet. The pins lean on the lamination surface of the upper pole and the whole assembly is designed in such a way that the table and the symmetry plane of the magnet are parallel. A Taylor-Hobson sphere can be mounted on each slide.

The levelling screws of the magnet are adjusted to bring the magnet axis on an horizontal plane; in addition, we require that the table is levelled in the azimuthal direction with respect to the cylinder axis. The slides are then moved to align the sphere centres on the vertical plane passing through the mechanical axis of the magnet and the slide positions are registered. The vertical distances between the two sphere centres and the mechanical axis are measured. The positions of the Taylor-Hobson spheres with respect to the cylinder axis are known with an accuracy of ±40 μm in the horizontal plane and ±20 μm in the vertical one, and are shown in Table III as configuration #1.

The magnet was then positioned on the rotating coil system [1]. Preliminary results on the magnetic alignment exhibited a large azimuthal rotation (≈7mrad) of the magnetic horizontal symmetry plane with respect to the mechanical one, defined by the alignment table on top of the magnet. We repeated therefore the mechanical alignment with a second set of pins, which lean on the iron plate welded on top of the laminations instead of the lamination surface (configuration #2): we found that in this case the rotation of the magnetic symmetry plane with respect to the mechanical one was less than 1 mrad.

It can be seen from Table III that the uncertainty in the symmetry plane position makes the measurement of the distance between mechanical and magnetic axes unreliable. We have asked therefore the supplier to undertake his actions to give us a reliable definition of the reference surface for the alignment pins. The measurements will be then repeated.

Table III - Mechanical positions of the reference spheres

Configuration #1	Vertical distance [mm]	side A side B	500.90 500.92
	Slide position [mm]	side A side B	8.96 15.39
Configuration #2	Vertical distance [mm]	side A side B	500.13 500.24
	Slide position [mm]	side A side B	12.40 12.00

The relative positions of the six poles have been verified by measuring the coordinates of 24 points along the pole profiles, two for each pole face. The coordinates were computed from angular measurements taken with two theodolites, connected to a computer and managed by a special program (ECDS3 from LEICA). The results are shown in Fig. 16. The measured values are consistent with the required tolerances.

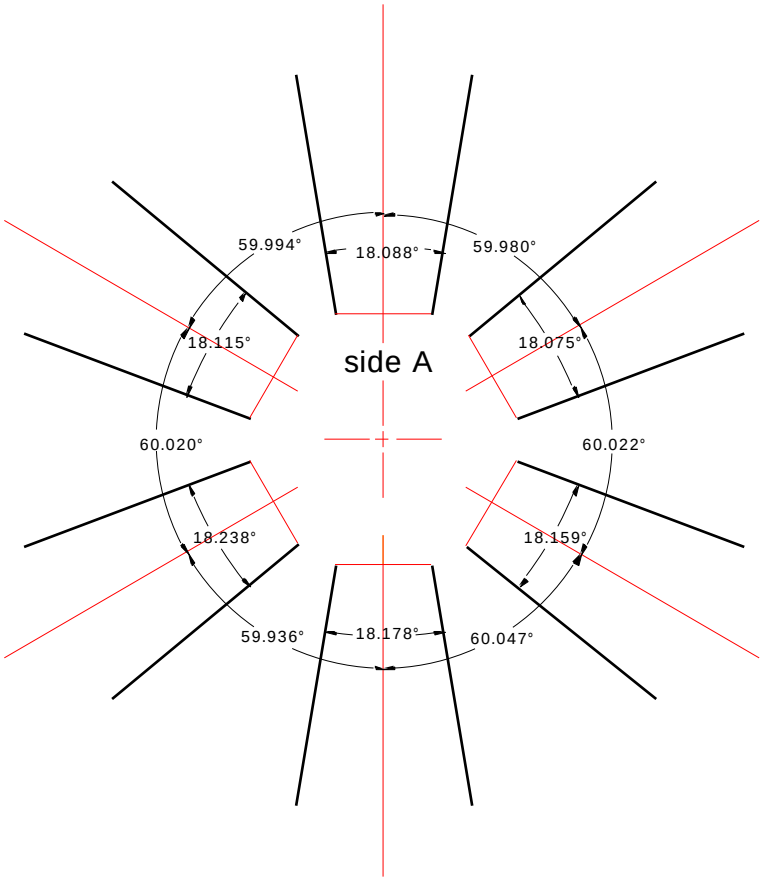

Figure 16. Angles between poles.

References

1 F. Iungo, M. Modena, Q. Qiao, C. Sanelli "DAΦNE magnetic measurements systems" - DAΦNE Technical Note MM-1 (2/12/94).

2 B. Bolli, F. Iungo, F. Losciale, N. Ganlin, M. Preger, C. Sanelli, F. Sardone "Field quality of the small quadrupoles for the DAΦNE Main Rings" - DAΦNE Technical Note MM-10 (22/2/96).